Examination of a Site-Specific, Physics-Based Seismic Hazard Analysis, Applied to Surrounding Communities of The Geysers Geothermal Development Area

Lawrence Hutchings[1], Jean Savy[2], Corinne Bachmann[1], Oliver Heidbach[3], Mamun Miah[4], Nate Lindsey[1], Ankit Singh[1], and Roselyne Laboso[5]

[1]Lawrence Berkeley National Laboratory, Earth Sciences Division, Berkeley California
[2]Consultant
[3]Helmholtz Centre Potsdam, GFZ German Research Centre for Geosciences
[4]University of Mississippi, Oxford, Mississippi
[5]Temple University, Philadelphia, Pennsylvania
ljhutchings@lbl.gov

Keywords

Seismic hazard, The Geysers, Geysers communities, physics-based PSHA, conventional PSHA, induced seismicity

ABSTRACT

We examine an approach to calculate seismic hazard from induced seismicity based on physics-based computations. This is done through the formal statistical process commonly referred to as probabilistic seismic hazard analysis (PSHA). We also examine a means to extend computations to a site-specific map for an entire region. Seismic hazard was estimated for a 50 km radius area centered on The Geysers, California. We performed both a traditional PSHA and a physics-based PSHA. We calculated hazard curves at 61 sites in the study area. Ambient noise samples were collected at these sites to modify calculations for site specific information. Further, twenty-three surface geologic units were identified within the study area and site specific calculations were extended to the entire region by interpolation along these geologic units. We first applied the conventional approach by using the actual catalog of the past ten years of earthquakes to estimate the hazard over this period; and thus, the sources of earthquakes were the actual fractures and faults, the rate of occurrence was the actual rate. We then applied an attenuation relation derived with The Geysers data to calculate hazard. In the physics-based approach, the same elements of the PSHA were employed, except physics-based calculations were used to calculate the hazard for the same ten year period. Sources of earthquakes were known faults and random fractures, and the occurrence of earthquakes was determined by geomechanical modeling of the distribution of stress and pressure in the development area. Ground motion was calculated from simulated earthquake ruptures and calculations of wave propagation instead of attenuation relations. We did not distinguish between induced and natural events in either study.

Hazard maps of the number of occurrences of two levels of ground motions over a ten and one year period were developed for values greater than or equal to 0.0014g and 0.1g, respectively. These are generally identified as the minimum level at which humans detect ground shaking and the minimum level at which damage to structures can occur, respectively. For the area within a 50 km radius of The Geysers, the estimated occurrences of the lower level of ground shaking exceeded 8 per year at some locations adjacent to the reservoir development area and diminished to near zero at greater distances. For the same region the estimated occurrences of the 0.1 g or greater was 0.4 per year (approximately once every 2.5 years) adjacent to the reservoir region and diminished to near-zero at greater distances. Remarkably, it was found that calculations by both conventional and physics-based approaches provided very similar results. This is very surprising since they were calculated by completely independent means. Consequently, the calculation of the conventional approach, based on actual data, provides confidence in the physics-based approach used.

Introduction

We examine an approach to calculate seismic hazard from induced seismicity based on physics-based computations. This is done through the formal statistical process commonly referred to as probabilistic seismic hazard analysis (PSHA). We also examine a means to extend computations to a site-specific map for an entire region. We map the seismic hazard for a 50 km radius area centered on The Geysers, California (Figure 1). We only address locations outside The Geysers development area. This is a research effort and not intended as a commercial PSHA.

The basic approach of a PSHA is to create a catalog of future earthquakes and estimate the ground motion at particular sites from the earthquake records. PSHA has historically been estimated for naturally-occurring tectonic earthquakes. In the current study, PSHA is extended to include induced earthquakes and hazard is calculated with both a conventional and physics-based approach. Only sources within the The Geysers geothermal volume (TGGV) are considered.

To test the physics-based approach, we used the actual catalog of the past ten years of earthquakes and ground motion attenuation relations to estimate the hazard with a conventional PSHA and compared it to physics-based PSHA over the same period. In the physics-based approach a catalog of earthquakes was created through geomechanical modeling and ground motion was calculated from simulated fault rupture and wave propagation.

Hazard maps of the number of occurrences of two levels of ground motions over a ten and one year period were developed for values greater than or equal to 0.0014 g and 0.1 g, respectively. These are generally identified as the minimum level at which humans detect ground shaking (National Academy, 2012; DOE, Wald et al., 1999) and the minimum level at which damage to structures can occur (NIESE, 2010), respectively. These are hazard maps; whether or not they disturb people or cause damage depends upon a fragility function to estimate the risk. That is not part of this study.

Two good reasons to utilize a physics-based approach are the use of fragility functions and the need to calculate hazard for conditions that have not occurred in the past. If conditions change in the future, it would not be appropriate to calculate hazard based upon seismicity from the past. The physics-based approach models the expected conditions for the future. The second benefit of a physics-based approach is in the way fragility functions are used. Fragility functions translate the seismic hazard to consequences; i.e. annoyance to humans or damage to structures. Traditional fragility functions utilize the single parameter of the hazard curve, usually peak acceleration or spectral acceleration, and estimate the consequences in terms of damage to classes of structures or human response. In reality fragility is dependent upon amplitude, frequency content and duration of ground shaking and requires a full time history to be fully assessed. Conventional risk studies generally seek time histories to match a single parameter amplitude, expected frequency content and duration of ground shaking to determine the fragility of critical facilities. The physics-based approach generates the time histories directly from the study, and it is therefore easy to include fragility functions that account for realistic time histories as part of the calculations.

The choice to include a very low level of ground shaking in the hazard calculation dictates that the analysis extends to smaller magnitudes than the M 4.5 normally considered in conventional PSHA, and to the shorter periods of surface ground motion shaking generated by nearby earthquakes. We limited the study to earthquakes with M > 2, since smaller events will not propagate significant energy outside of The Geysers development area. We did not distinguish between induced and natural events in either study. Rather, we calculated the occurrence of earthquakes in the area from the physical conditions that can cause either induced or tectonic events, or utilized the history which includes both induced and tectonic events.

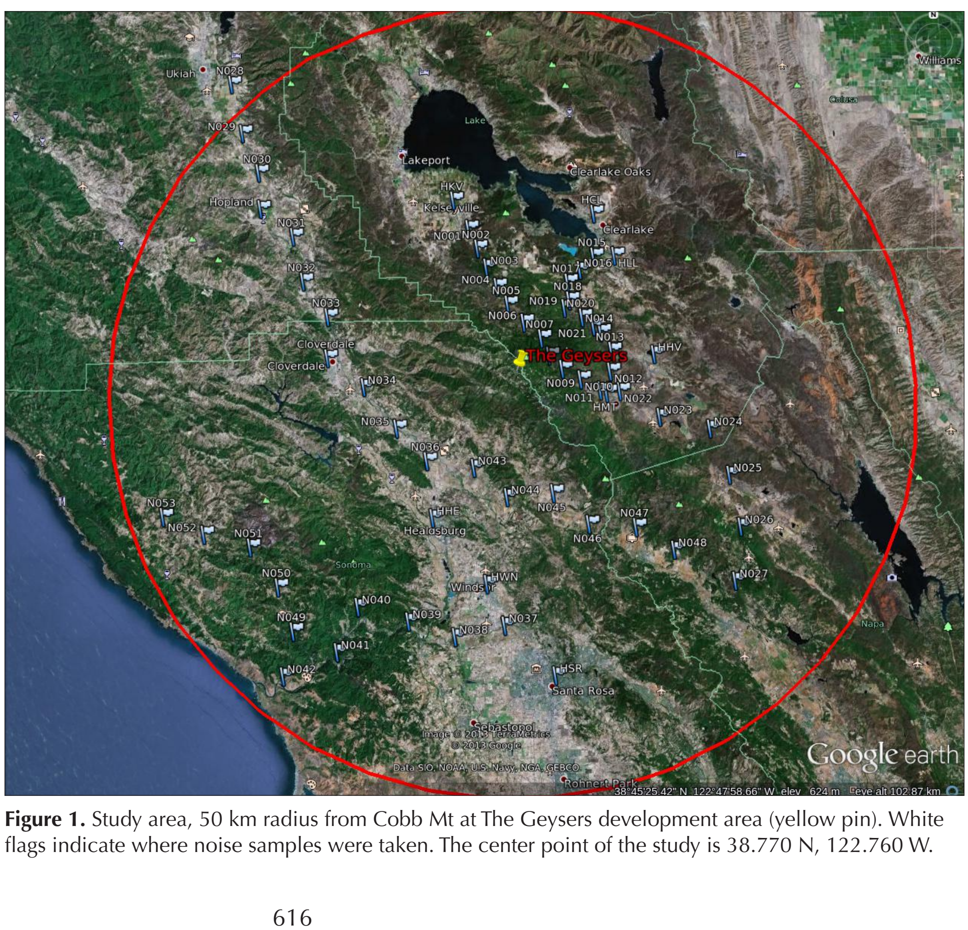

Figure 1. Study area, 50 km radius from Cobb Mt at The Geysers development area (yellow pin). White flags indicate where noise samples were taken. The center point of the study is 38.770 N, 122.760 W.

With the physics-based approach, we utilize the work of Altmann et al. (2013) and Bachmann et al. (2012). Altmann et al. utilize a thermo-hydro-geomechanical numerical model to calculate stress changes due to injection and extraction of fluids, thermal stresses, tectonic loading and fault slip of M > 4 earthquakes, calibrated to observations. Further, for this project Heidbach and Altmann (personal communication, 2013) calculated pressure as a function of position throughout TGGV for the next 25 years. We subsequently use another geo-mechanical modeling code (Bachmann *et al.*, 2012) to calculate the number of earthquakes that will occur.

In both standard and physics-based PSHA we utilize the computer program SimRisk (Jean Savy, personnel communication, 2014) to calculate hazard. SimRisk calculates hazard for non-stationary physical processes. Thus, the products of the calculations are hazard curves that give annual probabilities for a selected set of windows in time. SimRisk uses simulated and historic catalogs of earthquakes. Catalogs can be calibrated to ensure that the regional seismic moment is consistent with an existing ground-truth catalog if available. Ground-motion is calculated with either attenuation relationships or simulation of earthquake rupture and calculation of wave propagation. In either option, sets of ground motion inputs can be used to account for epistemic uncertainty.

Site Specific Calculations

For both conventional and physics-based PSHA the hazard is calculated at 61 sites in the region surrounding TGGV, primarily in the center of commercial and residential areas. We collected ambient noise samples at these sites in order to modify calculations for site specific information. We extend site-specific calculations to the entire region by interpolation along similar geologic units.

Geologic Units

The area outside of TGGV is mainly composed of rocks of the Franciscan Complex, Coast Range ophiolite, and the Great Valley Sequence (Jayko and Blake, 1984). The Franciscan Complex, a greywacke unit covers most of the Coast Ranges of California and can be subdivided to coastal, central, and eastern belts (Blake et al., 1988; Jayko and Blake, 1989; Jennings, 1977; McLaughlin et al., 1988). The Coast Range ophiolite is composed of ultramafic, mafic, and minor felsic igneous rocks of the late Mesozoic upon which Jurassic and Cretaceous strata of the Great Valley Sequence were deposited (Bailey et al., 1970). Twenty-three geologic units have been identified within a 50 km radius of TGGV (Jennings et al., 1977), which are shown in Figure 2. These units are utilized below as separate site response areas when performing hazard mapping. Identification of units is available in Jennings et al., 1977. Table A1, Appendix lists the geologic unit for each recording site.

Incorporating Noise Measurements

Near-surface geology is known to have a significant effect on propagating seismic energy, which is generally referred to as site response. Near surface amplification of earthquake ground motion is well documented (Abercrombie, 1997; Ioannidou et al., 2001; Baise et al., 2001), and can directly result in greater earthquake damage (Singh et al., 1988; EERC, 1990; Hutchings and Jarpe, 1996). We apply this principle to modify hazard calculations. Here we assume that each surface geologic unit is more similar within the unit than with other geologies, so we extrapolate within each unit. We took noise samples on competent geology and not on thick soil deposits, so results are for competent geology and modification for sites with thick soil deposits would have to be addressed on an individual basis.

Our basic assumption for estimating the effect of near surface geology on hazard calculations is that seismic noise is amplified by near surface geology in the same way as seismic signals from nearby earthquakes, for the same frequency band. In this case, noise refers to the vibrations from far distant sources, such as distant trains, oceans, forests, and distant earthquakes that collectively contribute a relatively constant level of earth vibrations. Local noise sources such a generators, traffic, people, or local trains are excluded. Following Nakamura (1989), ambient noise measurements

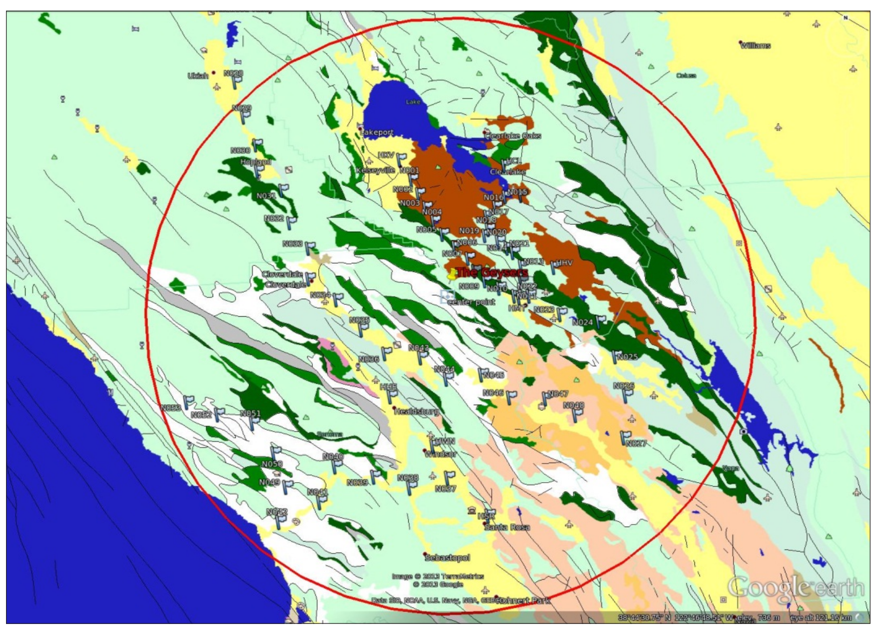

Figure 2. Geologic units near The Geysers. Flags show where noise measurements were taken.

have been widely used for site-specific investigations and in microzonation studies (e.g., Priolo et al., 2001; Scherbaum et al. 2003).

In this study we use a simple approach. First, we assume the noise has a "white" spectra, and is modified by the site response. We then band pass the ambient noise recordings between 1.0 and 25.0 Hz (the frequency band of our interest), and measure the time series amplitude levels in the time domain. We than assign a site amplification factor to the nearest whole number between 1 and 5, when compared to our sites with the lowest level of noise, which is assumed to be the most competent geologic formation.

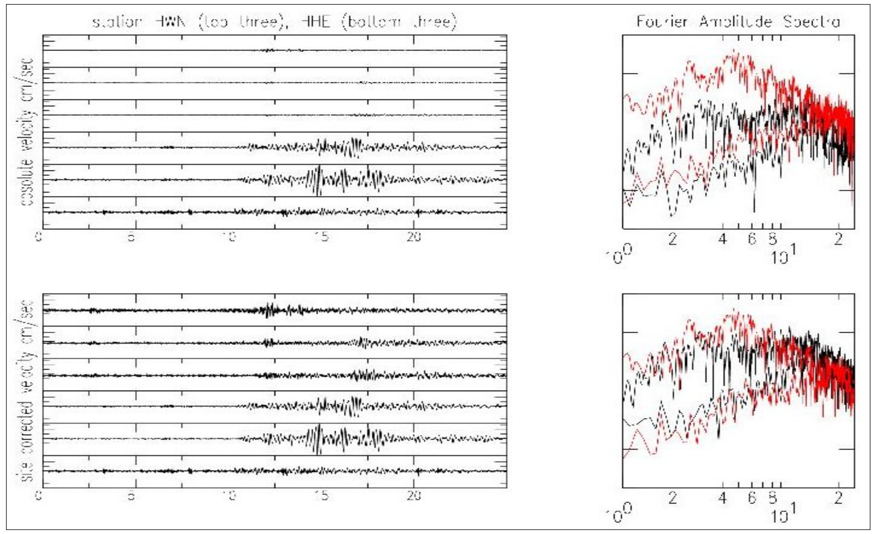

Figure 3. (top) Records at two stations recording the same earthquake and at the same distance. (bottom) shows the same recordings, but the three traces from the first site are normalized by the amplification factor.

Figure 3 (top) shows three-component recordings at two sites, band passed at 1.0 – 25.0 Hz (our hazard frequency range of interest) and plotted on the same vertical scale; on the right are the Fourier amplitude spectra of a common component. First, notice the shape of the spectra below the source corner frequency of the event is the same as the noise (i.e. they have the same slope). Now, the second set of records on the bottom shows the same recordings, but the three traces from the first site are normalized by the amplification factor; i.e., since the ambient noise was 5 times greater for the second site, the three records from the first site were multiplied by a factor of 5 to normalize to the same ambient noise level, and thus to normalize the earthquake recordings. This is done for demonstration purposes. In application, the reverse is done, i.e. sites with an amplification factor of 5 have hazard calculations multiplied by 5.

*Sesimic Hazard Map*s

The probabilistic hazard mapping methodology described herein provides a means to extrapolate and interpolate (referred to only as interpolation below) the hazard calculated at the 61 site-specific locations to the hazard throughout the 50 km radius. It is evident from Figure 2 that surface geology varies significantly within the 50 km radius area, which will affect the calculation of hazard. Although mapping software such as Generic Mapping Tools (GMT) can perform ground motion interpolation using its built-in programs, it cannot reflect the surface geology during the gridding process (grid points lie on different soil types).

Our technique is to interpolate the hazard estimates within the same kind of geologic units since they presumably will have similar amplification factors, as discussed previously. This procedure, of course, assumes that we have at least one recording for each kind of geologic unit. Once we have one hazard calculation for one site within a geologic unit, then all of the grid points within that unit will be interpolated in finely gridded points. If more than one site was sampled in a unit (and they sometimes do not all have the same value), interpolation within the unit is weighted by distance from each data point. In addition, interpolation assumes a 1/R fall-off or increase in the calculated values.

Conventional Probabilistic Seismic Hazard Analysis (PSHA)

Generally, for conventional PSHA, in the *first step*, the sources of earthquakes are identified as within zones where events occur along randomly oriented fractures or along specific faults. Tectonic stresses are regulated by the movement of tectonic plates that generate small and large earthquakes that are assumed to occur at a predictable long-term rate. This is traditionally described by a Gutenberg-Richter recurrence relationship for the number of events as a function of magnitude: Log N = a – b M. Where, *N* is the number of earthquakes per year greater than or equal to magnitude *M*, the slope is the *b*-value, and *a* is the intercept value for number of earthquakes with 0 magnitude. Generally, different *a* and *b*-values are identified, from historic catalogs of previous earthquakes, for all sources of earthquakes, including induced events. The sources and their *a*- and *b*-values are used to create a catalog of all the earthquakes that can affect a site for a period of time. This is *step two* in a hazard calculation. Ground motion prediction equations (attenuation relations) are used for *step three* to calculate the ground motions produced by the earthquakes at sites of interest. Usually, ground motion is described as a single hazard parameter, such as peak acceleration or the spectral response at a particular frequency. This provides a catalog of all the occurrences of the hazard parameter expected to occur for a period of time. In *step four*, a hazard curve is calculated by integrating the occurrences of the hazard parameter, which provides an estimate of the likelihood of exceedance of the parameter per year. Each time a different catalog of hazard parameters is produced by varying the estimates for *steps* 1 through 3, a different hazard curve is calculated. The average of these curves is typically used to provide the hazard estimate. Hazard can be converted to risk by fragility functions that relate the hazard parameter to the effect on people or structures. Finally, the hazard or risk at each location is interpolated to provide a hazard or risk map.

Sources of Earthquakes

We only consider the sources of earthquakes within and bounding TGGV for the hazard calculations. Two major right-lateral faults of the greater San Andreas transform fault system bound the geothermal field: the inactive Big Sulphur Creek/Mercuryville Fault zone to the SW (Hartline, Calpine, personnel communication, 2015), and the Collayomi fault to the east (McLaughlin, 1981; Allis, 1982; Donnelly-Nolan et al., 1993, Boyle et al., 2011). Only the Cobb Mountain fault (Thomas et al., 1981; McLaughlin, 1977) lies within TGGV. Several authors argue that the general area of Clear Lake, where TGGV is located, is under extension (Donnelly-Nolan et al., 1993; Bufe et al., 1981; Oppenheimer, 1986; Eberhart-Philips, 1986; Allis and Shook, 1999). However, mapped faults are primarily strike slip.

Altmann et al. (2013) included the Maacama, Collayomi, and Cobb Mountain faults in their geomechanical model. Other known faults outside TGGV, but within their model are two branches of the Wight Way fault and two branches of the Geyser Peak fault. The only fault where they calculated significant stress changes is the Cobb Mountain fault. These stress changes bring this fault, and the bounding faults, farther from failure. In view of these results, we consider any large earthquakes along the Cobb Mountain- and bounding faults, if they occur, to be caused by normal tectonic processes and not induced from injection. Still, our study does allow for earthquakes up to the maximum magnitude to occur along these faults. However, such earthquakes have very long return periods and are not likely to occur within the next ten years, and add very little to the hazard calculation.

Many small earthquakes occur within and near the steam reservoir on randomly oriented fractures. The Geysers steam reservoir lies primarily within a fractured metagreywacke in steeply dipping packets (Thompson, 1992). Granitic intrusions into the metagreywacke atarting about 1.2 Ma led to the formation of the felsite layer (Brikowski, 2001; Schmitt et al., 2003; Schriener and Suemnicht, 1980), which is the source of heat for the geothermal system. The shallowest felsite encounter is in the central and southeastern parts of the field at 0.7 km depth, and deepens towards the northwest to 2.5 km depth (Thomas, 1981; Sternfield, 1989; Brikowski, 2001; Boyle et al., 2011). The natural heat produced from the felsite leads to the presence of fumaroles and hot springs that appear on the surface.

Rate of Earthquakes

For the conventional PSHA we use the catalog of earthquakes for the past ten years for the hazard calculation for $M < 4.5$ earthquakes; thus, *a*- and *b*-values are naturally included in the estimate of the seismicity. This includes both tectonic and induced seismicity. Large tectonic earthquakes along the Maacama, Collayomi and Cobb Mountain faults are very rare events and do not appear in the catalogs due to the very short time period of the hazard calculation. Further, the stress changes along the Maacama and Collayomi faults are so small that calculated induced earthquakes along these faults do not appear in the catalogs either. From geomechanical modeling, we assume large induced earthquakes can occur along the Cobb Mountain fault. These are included as characteristic events. Still, their rate is so low that they do not affect the calculation of the number of occurrences of either the low or higher level of ground motion addressed in this report.

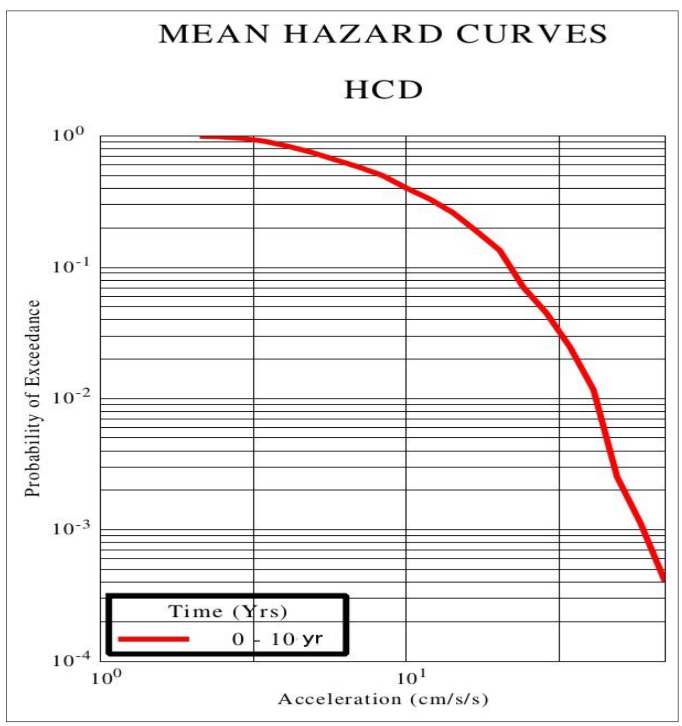

Figure 4. Hazard curve at site HCD. Hazard calculations for each site were modified by the site-specific information.

Attenuation Relations

Attenuation relations, often called ground motion prediction equations (GMPEs), are generally derived by regression of worldwide strong motion data (e.g., Abrahamson et al, 2003). Generally, GMPEs do not extend to magnitudes below 4.5 - 5, and even then are very poorly constrained for the smallest events and short distances

Figure 5. Color coded contour map of the number occurrences of 0.0014 g or greater per ten years within a 50 km area of TGGV (black circle). White areas exceed the range of the scale.

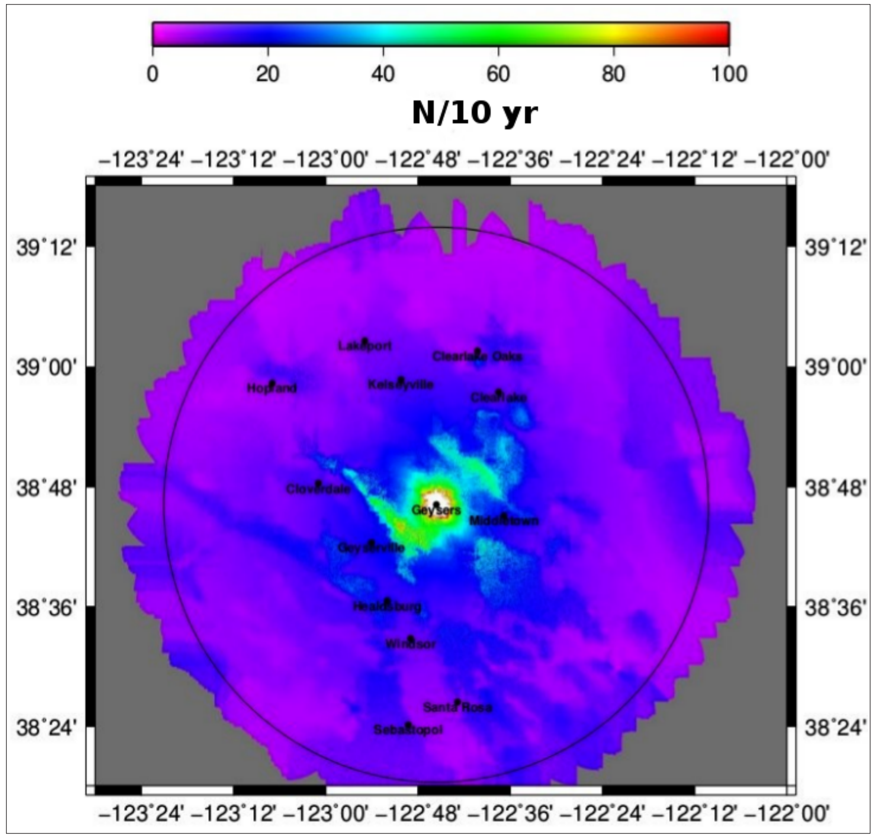

(e.g., Bommer et al., 2006). For *step three* (above), we use the ground motion attenuation relations of Douglas et al. (2013). Douglas et al. (2013) developed GMPE's specifically for magnitudes less than 3.5 and short distances, based on data from six geothermal areas. Douglas et al. data from The Geysers are centered along his relationship, and we therefore conclude that the Douglas et al. (2013) relationship is adequate for the average site conditions at The Geysers. We modify the estimated values from this relationship with site specific information to modify the hazard calculations.

Site Specific Hazard

A hazard curve provides an estimation of the likely annual probability of exceeding for given values of a hazard parameter. Typically, peak ground acceleration is chosen as the hazard parameter (and our chosen hazard parameter for this study). The ordinate of the hazard is the likelihood of exceedance and the abscissa is the level of hazard parameter. The hazard curve is normalized to probability of exceedance per year. Figure 4 shows a mean hazard curve at one site (HCD) for the conventional PSHA. The amplification factor for this site is 1.0. These calculations are made for each site. Table A1, Appendix. See Hutchings et al., (2014) for details on the hazard calculation

Hazard Maps

Figure 5 shows a color-coded contour map of number of occurrences of the low level of acceleration (0.0014 g) per ten years within a 50 km radius of TGGV, derived from the mean hazard curves at 61 sites. Figure 6 shows a color-coded contour map of the decimal likelihood of the higher ground motion of 0.1g or greater occurring each year. The small white section in the center of the maps are areas that exceed the range of the scale shown, primarily in TGGV. Table A1 lists the number of the low level ground motion expected for ten years

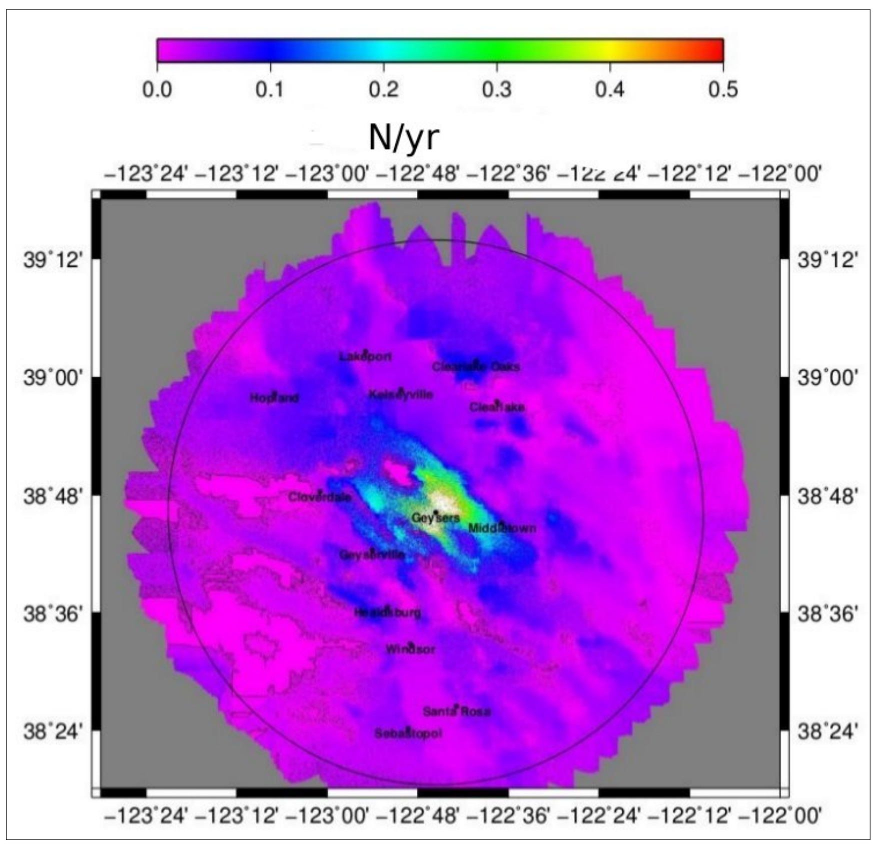

Figure 6. Color coded contour map of the decimal likelihood of 0.10 g or greater acceleration per year within a 50 km area of TGGV (black circle). White areas exceed the scale range.

and the decimal likelihood of the higher level occurring each year at the 61 sites. These values are interpolated to create the maps. Both hazard values are statistically expected, but may not occur exactly at these rates. Rather over several time periods the number would average out to be the expected value. Figure 5 indicates that there are over 80 low level occurrences per ten years at some locations adjacent to TGGV; this number diminishes to zero at greater distances. Figure 6 indicates that there is a 0.4 likelihood per year, or approximately 4 occurrences in ten years, of 0.10 g or greater adjacent to TGGV and diminishes to zero at greater distances.

Calculation of Ground Motion Hazard (Physically-Based Hazard Calculation)

Heidbach and Altmann (personal communication, 2013) built a 3D thermo-hydro-geomechanical numerical model of TGGV and calculated pressure evolution throughout TGGV from 1960-2037. The model accounts for the far-field tectonic loading and co-seismic stress changes from the M > 4 events, as well as for the pore pressure and thermal stress changes due to fluid extraction and re-injection in TGGV. After the implementation of an initial stress state that is calibrated against data for the orientations of maximum horizontal stress and stress regime from earthquake focal mechanism solutions, they apply kinematic far-field boundary conditions derived from continuous GPS stations. We utilize their calculation for the next ten years (i.e., 2014 - 2024), based upon the assumption that injection wells present today are a good estimate of the wells in place for the next ten years. Pressure is obtained for a 300 m grid spacing, while time steps are six months. The production and re-injection rates are assumed to remain constant at present levels.

We use a geomechanical program as implemented by Bachmann et al. (2012) and Goertz-Allman and Wiemer (2013) to convert pore pressure changes from the thermo-hydro-geomechanical numerical model of Heidbach and Altmann (per. comm. 2013) into a synthetic catalog of induced earthquakes for the hazard calculation. The program randomly distributes potential failure points in the three-dimensional volume, representing pre-stressed faults or fractures, and analytically calculates the Mohr-Coulomb diagram, and thus a failure criterion for each failure point. Earthquakes are induced as a result of failure due to effective stress changes caused by the pore-pressure changes. Up to this point, the method is similar to the earlier work of Shapiro et al (2007). However, Shapiro et al. did not determine event magnitudes, which are a critical element for hazard analysis.

The program uses an inverse relationship between *b*-values and the differential stress, found in laboratory studies and for natural events (Amitrano, 2003, Schorlemmer et al, 2005), to determine the *b*-values of an induced event as described by Bachmann (2011). This is based on the two papers by Bachmann et al. (2012) and by Goertz-Allmann and Wiemer (2013). A magnitude is randomly drawn out of this specific distribution.

Hazard Calculation

We generated 20 catalogs with Bachmann's approach by varying input parameters to the failure models. We use a constant coefficient of friction for all failure points for one run, but varied it for different runs. *b*-values were used to identify the magnitude of an event. The minimum and maximum principal stresses are based on a background stress regime. We use the same value for the whole volume, but vary them for different calculations. We utilized synthetic Green's functions to calculate the ground motion, for a total of 20 hazard curves. Figure 7 shows the mean and three different standard deviations of the hazard curves at one station. See Hutchings et al. (2014) for details on the hazard calculations.

Hazard Maps

Figure 8 shows a color-coded contour map of number of occurrences of the low level of acceleration per ten years (0.0014 g) within a 50 km radius of TGGV. Individual values calculated for sites where noise samples were taken are listed in Table A1. Figure 9 shows a color-coded contour map of the decimal likelihood of a ground motion of 0.1g or greater occurring each year (also listed in Table A1 for each selected sites). As discussed, for example, an occurrence of 0.1 means there

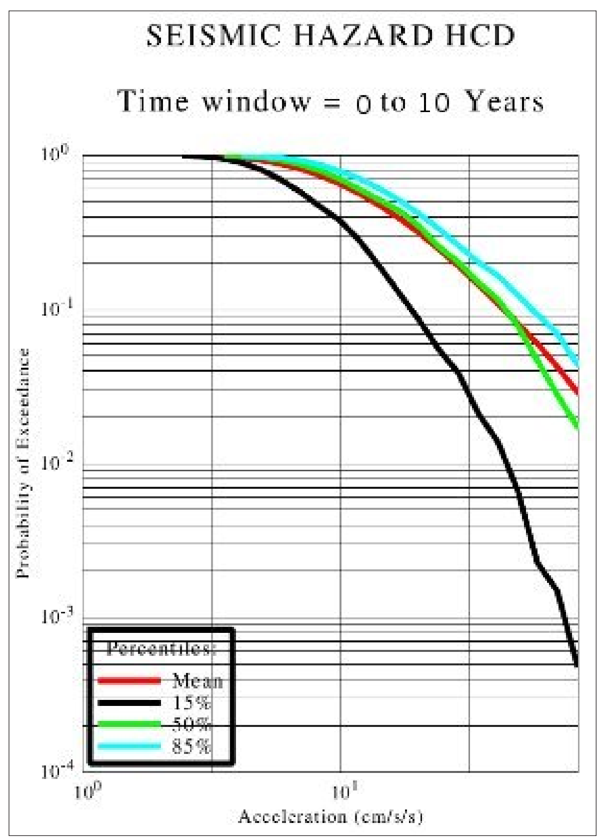

Figure 7. Hazard curve at site HCD normalized for exceedance per year. Hazard calculations for each site were modified by the site-specific information.

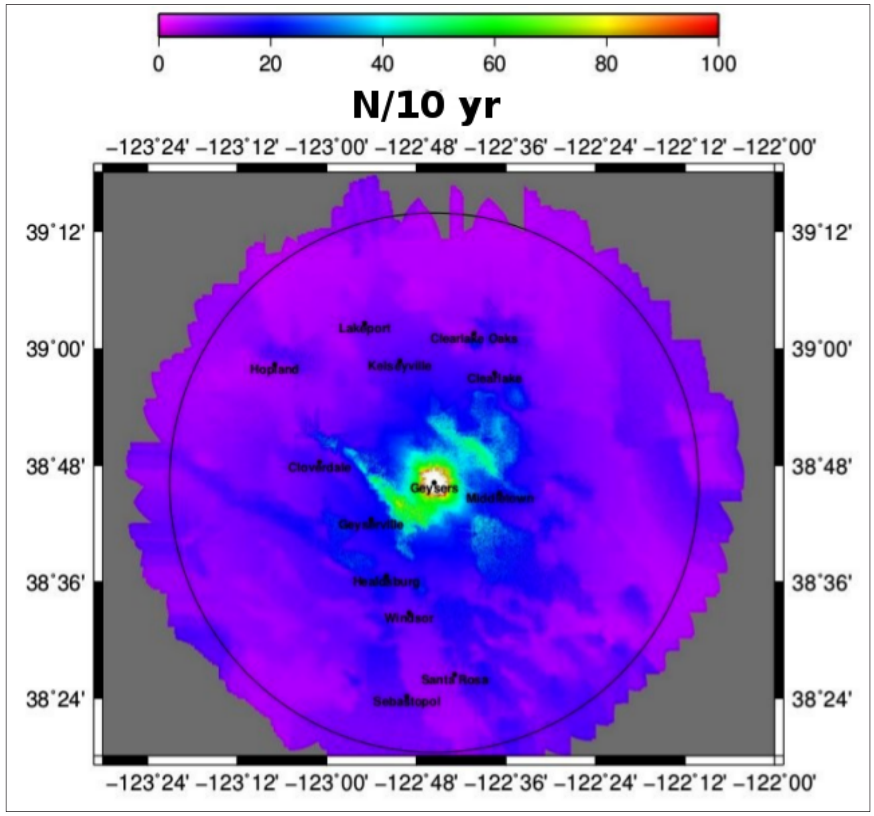

Figure 8. Color coded contour map of the number occurrences of 0.014 g (N/yr) within a 50 km area of TGGA (black circle). White areas exceed the scale range.

is one chance in 10 of occurring each year, but not necessarily one will occur each ten year period. Figure 9 shows more site-specific detail than Figure 7 because the scale has been changed from 0.0 - 0.5 to 0.0 - 0.1. White areas exceed the range of the scale shown. It is apparent from Table A1 that values from the physics-based approach are very similar to those from the conventional approach, which would produce a map very similar to Figure 7 if they had the same scale. Figure 9 would also show 0.10 g or greater occurring approximately seven times in ten years adjacent to TGGV, close to what was observed for the conventional study. Here we want to show the site-to-site variability. Figure 8 shows the low level of acceleration values are exceeded over 80 times per ten years at some locations adjacent to TGGV, similar to what was observed for the conventional PSHA study.

Discussion and Conclusions

We examine an approach to calculate seismic hazard from induced seismicity based on physics-based computations. We modified the conventional PSHA to allow for physics-based computations to address stress changes, and therefore seismicity changes, in the future. We also developed a methodology to create hazard maps for a region. We compared our results to a conventional PSHA based upon actual recordings of earthquakes over a ten year period. The hazard is calculated at 61 sites in the region surrounding to The Geysers. Hazard calculations were modified to be site-specific. First, noise measurements were obtained at the 61 sites and amplification factors for site geology were estimated. Then, 23 surface geologic units were identified. A complete hazard map is obtained by interpolating calculations within similar surface geologic units. The geology and noise samples are for competent geology, so the hazard maps are for competent geology.

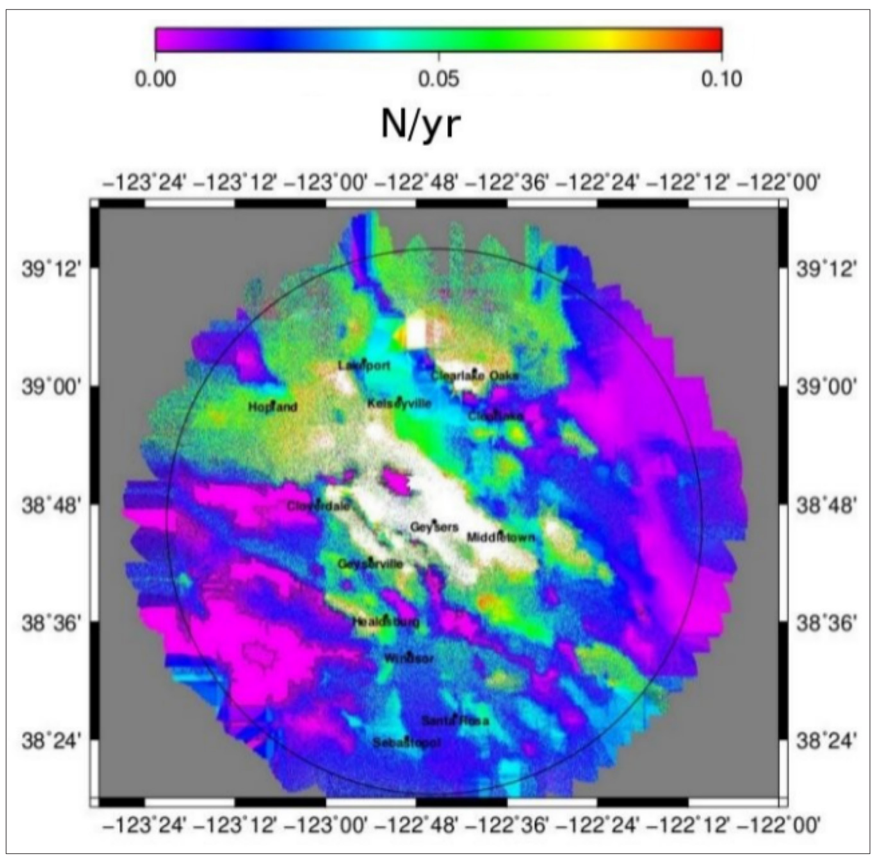

Figure 9. Color coded contour map of the decimal likely number of 0.10 g or greater occurring per year within a 50 km area of TGGA. White areas exceed the scale range. This figure shows more site-specific details than Figure 6 because the scale has been changed to 0.0 to 0.1.

One of the main results of this study is that the classical approach to PSHA and the physics-based approach provide provide very similar results. This is evident by comparing the maps show in Figure 5 and 8 and values listed in Table A1. Table A1 lists the calculated values of number of occurrences of the lower and higher levels of ground shaking at each of the 61 sites used in this study, and for the two approaches. Comparing these values provides the best example of how similar the results are. Figures 6 and 9 would show the same effect, but rather than show two maps that are almost identical, we changed the scale for Figure 9. This better shows the variability in mapping we obtain by using site-specific geologic information.

For both studies, the estimated occurrences of the lower level of ground shaking exceeded 80 per ten years at some locations adjacent to the reservoir development area and diminished to near zero at greater distances. For the same region the estimated occurrences of the 0.1 g or greater was 0.4 per year (approximately 4 every 10 years) adjacent to the reservoir region and diminished to near zero at greater distances. These estimates are for competent geology and numbers would change for sites with thick soil deposits.

It is somewhat surprising that the two approaches examined in this study give such similar results since they were calculated by completely independent means. The conventional approach used the actual catalog of the past ten years, while the physics-based approach used geotechnical modeling to calculate the catalog for ten years. Similarly, for the conventional PSHA, we utilized attenuation relations from past earthquakes recorded at The Geysers to translate the ground motion from the source to the site, while for the physics-based approach we calculated ground motion from simulated actual earthquake ruptures wave propagation. Finally, the sources of earthquakes were the actual sources for the conventional PSHA and identified faults and randomly distributed fractures for the physics-based approach. Since the conventional approach was based on the actual hazard for the past 10 years, we consider that matching the calculation of the conventional approach provides confidence in the physics-based approach. Actual recordings of ground acceleration at several locations throughout the study area would help validate the calculations and the mapping methodology.

Acknowledgement

We appreciate careful reviews from Patrick Dobson and Ernie Majer (Lawrence Berkeley National Laboratory) and Craig Hartline (Calpine-Geysers, Middletown, California). In addition DOE Award No. DE-EE0002756 provided funding, and we benefited from project leadership by Roland Gritto, ARRAY Technologies.

References

Abrahamson, N., G. Atkinson, D. Boore, Y. Bozorgnia, K. Campbell, B. C. Chiou, I. M. Idriss, W. Silva, and R. Youngs (2008). Comparisons of the NGA ground-motion relations, Earthq. Spectra 24, no. 1, 4–66.

Abercrombie, R.E. (1997) Near-surface attenuation and site effects from comparison of surface and deep borehole recordings, *Bull. Seismol. Soc. Am.* 87, 731–744.

Allis, R.G. (1982). Mechanism of induced seismicity at The Geysers geothermal reservoir, California, *Geophysical Research Letters*, 9(6), 629-632.

Allis, R. and Shook, G.M. (1999). An alternative mechanism for the formation of The Geysers vapor-dominated reservoir, *Proceedings of the 24th Workshop on Geothermal Reservoir Engineering, Stanford*, SGP-TR-162.

Altmann, Johannes B., Oliver Heidbach and Roland Gritto (2013) Relative Importance of Processes Leading to Stress Changes in The Geysers Geothermal Area. PROCEEDINGS, Thirty-Eighth Workshop on Geothermal Reservoir Engineering. Stanford University, Stanford, California, February 11-13, 2013. SGP-TR-198.

Amitrano, D., 2003, Brittle-ductile transition and associated seismicity: Experimental and numerical studies and relationship with the b value, Journal of Geophysical Research, 108, doi: 10.1029/2001JB000680.

Bachmann, Corinne Elisabeth (2011) New approaches towards understanding and forecasting induced seismicity. DISS. ETH NO. 19906. ETH, Zurich, Switzerland.

Bachmann, C.E., S. Wiemer, B.P. Goertz-Allmann and J. Woessner (2012) Influence of pore-pressure on the event-size distribution of induced earthquakes. *Geo Res Let,* 39, L09303-L09302.

Bailey, E.H., Blake, MC., Jr. and Jones, D.L. (1970). On-land Mesozoic oceanic crust in California Coast Ranges. U.S. Geol. Surv., Prof. Pap., 700-C: C70-C81.

Baise, Laurie, Lawrence Hutchings, and Steven Glaser (2001) Analysis of Site Response at Yerba Buena Island, San Francisco Bay, California from Weak Motion Recordings. Special Issue on Site Response, *Bollettino di Geofisica teorica ed applicata*, 42 219-243. Trieste, Italy.

Blake Jr., M.C., Jayko, A.S., McLaughlin, R.J., Underwood, M.B. (1988). Metamorphic and tectonic evolution of the Franciscan complex, northern California. In: Ernst, W.G. (Ed.), Metamorphism and Crustal Evolution of the Western United States.: Rubey, vol. VII. Prentice-Hall, Englewood Cliffs, NJ, pp. 1035–1060.

Bommer, J. J., and J. E. Alarcón (2006). The prediction and use of peak ground velocity, J. Earthq. Eng. 10, no. 1, 1–31.

Boyle, K., Jarpe, S., Hutchings, L., Saltiel, S., Peterson, J. and Majer, E. (2011). Preliminary investigation of an aseismic ‘doughnut hole’ region in the northwest Geysers, California, *Proceed. of the 36th Workshop on Geothermal Reservoir Engineering, Stanford,* SGP-TR-191.

Brikowski, T.H (2001) California geologic map data. http://mrdata.usgs.gov/geology /state/state.php?state=CA. Deep fluid circulation and isotopic alteration in The Geysers system: profile models, *Geothermics*, 30, 333-347.

Bufe, C.G., Marks, S.M., Lester, F.W, Ludwin, R.S. and Stickney, M.C. (1981). Seismicity of The Geysers-Clear lake region, *U.S. Geological Survey Professional Paper*, 1141, 129-137.

California geologic map data. http://mrdata.usgs.gov/geology/state/state.php?state=CA.

Calpine (2010) Calpine Enhanced Geothermal Systems Project, final Environmental Assessment. Prepared for: U.S. Department of Energy 1617 Cole Boulevard Golden, CO 8040, prepared by: RMT Inc., Calpine-Geysers, Middletown, June 2010.

Douglas, John, Benjamin Edwards, Vincenzo Convertito, Nitin Sharma, Anna Tramelli, Dirk KraJohn, Eaijpoel, Banu Mena Cabrera, Nils Maercklin, and Claudia Troise (2013) Predicting Ground Motion from Induced Earthquakes in Geothermal Areas. *Bul Seis Soc Am* 103, no. 3.

Donnelly-Nolan, J.M., Burns, M.G., Goff, F.E., Peters, E.K., and Thompson, J.M. (1993) The Geysers-Clear lake area, California: Thermal waters, mineralization, volcanism, and geothermal potential, *Economic Geology*, 88, 310-316.

Eberhart-Phillips (1986) Three-dimensional Velocity Structure in Northern California Coast Ranges from Inversion of Local Earthquake Arrival Times. *Bul Seis Soc Am* 76, no. 4, pp. 1025-1052.

EERC (1990). Preliminary report on the principal geotechnical aspects of the October 17, 1989, Loma Prieta earthquake, College of Engineering, University of California, Earthquake Engieering Research Center, Report no. UCB/EERC-90/05.

Goertz-Allmann, Bettina P., and Stefan Wiemer. “Geomechanical modeling of induced seismicity source parameters and implications for seismic hazard assessment.” *Geophysics* 78.1 (2012): KS25-KS39.

Heidbach, Oliver, Johannes B. Altmann (2014) Chapter 6; Towards the Understanding of Induced Seismicity in Enhanced Geothermal Systems. Final Report, Award No. DE-EE0002756, Performance Period: January, 29, 2010 through May 31, 2014.

Hutchings, Lawrence, Jean Savy, Corinne Bachmann, Oliver Heidbach, Mamun Miah, Nate Lindsey, Ankit Singh, and Roselyne Laboso (2014) Chapter 9; Towards the Understanding of Induced Seismicity in Enhanced Geothermal Systems. Final Report, Award No. DE-EE0002756, Performance Period: January, 29, 2010 through May 31, 2014.

Hutchings, L. and Wu, F. (1990) Empirical Green’s Functions from Small Earthquakes: A Waveform study of Locally Recorded Aftershocks of the 1971 San Fernando Earthquake. J Geophys Res, 95, 1187-1214.

Hutchings, L. and S. Jarpe (1996) Ground Motion Variability at the Highways 14 and I-5 Interchange in the Northern San Fernando Valley. *Bul Seis Soc Am* 86, no. 1B, pp S289-S299. UCRL-ID-121760.

Ioannidou, Eleni, Ioannis Kalogeras, Nicholas Voulgaris, Lawrence Hutchings, and George Stavrakakis (2001) Analysis of Site Response in the Athens Area from the 7 September 1999, Mw=5.9 Athens Earthquake and Aftershock Recordings, and Intensity. Special Issue on Site Response, *Bollettino di Geofisica teorica ed applicata* , 42, 183-208. Trieste, Italy.

Jayko, A.S., and Blake Jr., M.C. (1984). Sedimentary Petrology of Graywacke of the Fransiscan Complex in the Northern San Fransisco Bay Area, California: *in* Blake, M.C. Jr., ed., 1984, *Fransiscan Geology of Northern California: Pacific Section S.E.P.M.*, 43, 121-134.

Jayko, A.S., Blake Jr., M.C. (1989). Deformation of the Eastern Franciscan Belt, northern California. *Journal of Structural Geology*, 11, 375–390

Jennings, C.W., Strand, R.G., and Rogers, T.H. (1977). Geologic map of California: California Division of Mines and Geology, scale 1:750,000.

McLaughlin, R.J. (1977). The Franciscan Assemblage and Great Valley Sequence in the Geysers-Clear Lake Region of Northern California. File Trip Guide to the Geysers-Clear Lake Area. The Cordilleran Section of the Geological Society of America, April, 1977.

McLaughlin, R.J. (1981). Tectonic setting of pre-Tertiary rocks and its relation to geothermal resources in the Geysers-Clear Lake area, *U.S. Geol. Survey Professional Paper*, 1141, 3-23.

McLaughlin, R.J., Blake Jr., M.C., Griscom, A., Blome, C.D., Murchey, B. (1988). Tectonics of formation, translation, and dispersal of the Coast Range Ophiolite of California. *Tectonics,* 7, 1033–1055.

Nakamura, Y. (1989), “A Method for Dynamic Characteristics Estimation of Subsurface using Microtremor on the Ground Surface”, Quarterly Report of Railway Technical Research Institute (RTRI), Vol. 30, No.1.

National Academy, Committee on Induced Seismicity Potential in Energy Technologies (2012) Induced Seismicity Potential in Energy Technologies. The National Academies Press, Washington, D.C.

NIESE, National Information Service for Earthquake Engineering, 2010. http://nisee.berkeley.edu, Pacific Earthquake Engineering Research (PEER) Center, University of California, Berkeley.

Oppenheimer, Oliver HeidbachD.H. (1986). Extensional tectonics at The Geysers geothermal area, California, *Journal of Geophysical Research*, 91, B11, 11463-11476.

Priolo, E. A. Michelini, and L. Hutchings (2001); editors. Site Estimation from Observed Ground Motion Data. Bollettion Di Geofisica, teorica ed applicata, special edition Sep.-Dec., Vol 42.

Scherbaum F, Hinzen K-G, Ohrnberger M (2003) Determination of shallow shear wave velocity profiles in the Cologne, Germany area using ambient vibrations. Geoph J Int 152:597–612.

Schmitt, A.K., M. Grove, T.M. Harrison, O. Lovera, J. Hulen, and M. Walters (2003). The Geysers-Cobb Mountain magma system, California (Part 2): Timescales of pluton emplacement and implications for its thermal history. *Geochimica et Cosmochimica Acta*, 67, 3443-3458.

Schorlemmer, D., S. Wiemer, and M. Wyss (2005) Variations in earthquake-size distribution across different stress regimes: Nature, 437, doi: 10.1038/nature04094.

Shapiro, S. A., C. Dinske and J. Kummerow (2007) “Probability of a given-magnitude earthquake induced by a fluid injection” Geophy, Res. Let., 34 (22).

Soil Type and Shaking Hazard in the San Francisco Bay Area. http://earthquake.usgs.gov/regional/nca/soiltype/

Sternfeld, J. N. (1989). Lithologic influences on fracture permeability and the distribution of steam in the Northwest Geysers steam field, Sonoma County, California. Trans. *Geother. Resour. Counc*. 13, 473-479.

Surface geology based strong ground motion amplification factors for the San Francisco Bay and Los Angeles areas. http://peer.berkeley.edu/lifelines/lifelines_pre_2006/final_reports/Report_5B.pdf

Thomas, R. P., Rodger H. Chapman, and Herman Dykstra (1981). A Reservoir Assessment of the Geysers Geothermal Field. A.D. Stockton, Principal Investigator. California Department of Conservation, Division of Oil and Gas, Sacramento, Publication No. TR27.

Thomas, R. P. (1981). Subsurface geology. A reservoir assessment of The Geysers geothermal field. Calif. Div. Oil Gas Pub. No. TR 37.

Thompson, R. C. (1992). Structural stratigraphy and intrusive rocks at The Geysers geothermal field. *Geother. Res. Counc*. Special Report No. 17, 59-63.

Wald, D.J., V. Quitoriano, T.H. Heaton, H. Kanamori (1999) Relationshipsbetween Peak Acceleration, Peak Ground Veolcity, and Modified Mercalli Inensity in California. *Earthquake Spectra*, 15, pp. 557-564.

Table A1. Hazard calculations at 61 sites*.

						Classical PSHA w/site specific factor		Physically-Based w/site specific factor	
Site	**Latitude**	**Longitude**	**Dist.**	**Geologic Unit****	**Site Factor**	**number likely num occurrence per 10 yr >0.0014 g**	**annual likelihood damage hazard/yr >0.10 g**	**number likely num occurrence per 10 yr >0.0014 g**	**annual likelihood damage hazard/yr >0.10 g**
HCD	38 47.964	-123 01.060	22.6	Q	1	13	.00042	10	.00062
HCL	38 57.622	-122 38.083	23.7	QPc	1	12	.0099	9	.00013
HGU	38 30.208	-122 59.880	36.1	Q	2	20	0.0	8	0.0
HHE	38 36.973	-122 52.348	19.6	Q	4	~76	.0721	~84	.0691
HHV	38 47.811	-122 33.233	18.1	QPc	1	~13	0.0	~12	.0007
HKV	38 58.695	-122 50.217	24.1	Q	5	~110	.1631	~80	.2601
HLL	38 54.638	-122 36.390	20.5	Kl	1	~13	0.0	10	.0042
HMT	38 45.225	-122 37.375	12.1	Q	1	~17	.0081	~16	.0062
HSR	38 26.448	-122 42.255	36.9	Q	4	~44	0.0	20	0.0
HWN	38 32.548	-122 47.839	25.5	Q	1	~10	.0055	5	0.0
N001	38 56.685	-122 48.931	20.0	Q	5	~135	.4661	~70	.7871
N002	38 55.287	-122 48.193	17.2	Qv	1	~18	.0293	~17	.0502
N003	38 53.955	-122 47.454	14.6	Qv	1	~21	.0962	~19	.0771
N004	38 52.586	-122 46.586	11.9	um	1	~22	.2682	~19	.2677
N005	38 51.355	-122 45.667	9.5	Kjf	1	~23	.4682	~21	.7044
N006	38 50.091	-122 44.331	7.4	Kjf	1	~21	.5244	~20	.7356
N007	38 49.021	-122 42.875	6.5	Kjf	1	~23	.4082	~21	.7990
N008	38 47.808	-122 42.227	5.7	Kjf	1	~24	.3382	~22	.5292
N009	38 46.888	-122 41.136	6.6	Kjf	1	~21	.1993	~21	.2542
N010	38 46.173	-122 39.566	8.7	Kjf	1	~21	.0694	~19	.0835
N011	38 45.389	-122 37.900	11.2	Q	1	~18	.0142	~18	.0273
N012	38 46.700	-122 37.022	12.5	Ku	1	~17	.0115	~18	.0124
N013	38 48.088	-122 36.855	13.1	Ku	1	~17	.0079	~17	.0043
N014	38 49.373	-122 37.746	12.8	Ku	1	~17	.0188	~17	.0226
N015	38 54.616	-122 38.199	18.9	Kl	1	~14	.00098	10	.0019
N016	38 53.664	-122 39.409	16.5	Ku	1	~16	.0064	~13	.0052
N017	38 52.823	-122 40.492	14.3	Qv	1	~18	.0256	~15	.0248
N018	38 51.595	-122 40.392	12.5	J	1	~19	.0571	~17	.0524
N020	38 50.416	-122 39.328	12.0	J	1	~19	.0423	~17	.0546
N021	38 49.795	-122 38.349	12.4	Ku	1	~18	.0235	~18	.0488
N022	38 45.356	-122 36.264	13.6	J	1	~16	.0048	~17	.0041
N023	38 43.517	-122 32.920	19.0	Q	1	~12	0.0	10	.0035
N024	38 42.678	-122 28.667	25.4	um	1	10	0.0	9	0.0
N025	38 39.542	-122 27.171	29.4	Q	1	8	0.0	7	0.0
N026	38 30.663	-122 26.420	40.0	Kl	1	6	0.0	4	0.0
N027	38 32.476	-122 27.021	37.0	Tvp	1	5	0.0	2	0.0
N028	39 07.170	-123 09.584	50.0	Q	1	6	0.0	0	0.0
N030	39 00.860	-123 07.146	41.3	Q	1	8	0.0	4	0.0

N031	38 56.315	-123 04.1185	32.7	um	1	10	0.0	8	.0001
N032	38 53.210	-123 03.264	28.7	Kjf	1	10	0.0	10	.0009
N033	38 50.719	-123 01.127	24.0	Qls	1	~13	.00014	10	.0003
N034	38 45.899	-122 58.083	18.1	Q	1	~15	.0066	~12	.00697
N035	38 43.048	-122 55.318	15.2	Q	1	~16	.012	10	.0104
N036	38 40.852	-122 52.824	14.4	Q	5	~75	.0041	~85	.0043
N037	38 29.772	-122 46.425	30.4	Q	5	45	0.0	45	.0003
N038	38 29.086	-122 50.584	32.5	Q	1	8	0.0	2	0.0
N039	38 30.146	-122 54.461	32.4	TK	1	8	0.0	2	0.0
N040	38 31.169	-122 58.663	33.7	Q	1	8	0.0	2	0.0
N041	38 28.198	-123 00.431	39.7	Q	1	6	0.0	1	0.0
N042	38 26.686	-123 04.884	45.7	Q	1	4	0.0	1	0.0
N043	38 40.308	-122 48.776	11.8	Q	1	~16	.0079	~14	.0140
N044	38 38.305	-122 46.019	14.6	QPc	1	~13	.00028	~11	.0057
N045	38 38.530	-122 42.109	15.1	Q	1	~13	0.0	~12	.0038
N046	38 36.419	-122 39.166	20.4	TvP	1	10	0.0	9	.0038
N047	38 36.169	-122 35.220	23.9	Q	1	10	0.0	8	.000007
N048	38 34.589	-122 32.066	29.1	Q	1	9	0.0	5	0.0
N049	38 29.591	-123 04.105	40.8	Kjfm	1	6	0.0	1	0.0
N050	38 32.537	-123 05.345	38.2	Mzv	1	7	0.0	1	0.0
N051	38 35.197	-123 07.694	38.0	Kjfm	1	7	0.0	2	0.0
N052	38 36.097	-123 11.568	42.0	Kjfm	1	6	0.0	1	0.0
N053	38 37.301	-123 15.059	45.8	Kjfm	1	5	0.0	0	0.0

* missing station numbers had no data collected